

Chemical Science

Accepted Manuscript



This is an *Accepted Manuscript*, which has been through the Royal Society of Chemistry peer review process and has been accepted for publication.

Accepted Manuscripts are published online shortly after acceptance, before technical editing, formatting and proof reading. Using this free service, authors can make their results available to the community, in citable form, before we publish the edited article. We will replace this *Accepted Manuscript* with the edited and formatted *Advance Article* as soon as it is available.

You can find more information about *Accepted Manuscripts* in the [Information for Authors](#).

Please note that technical editing may introduce minor changes to the text and/or graphics, which may alter content. The journal's standard [Terms & Conditions](#) and the [Ethical guidelines](#) still apply. In no event shall the Royal Society of Chemistry be held responsible for any errors or omissions in this *Accepted Manuscript* or any consequences arising from the use of any information it contains.



Journal Name

ARTICLE

An Efficiently Tuned d-Orbital Occupation of IrO₂ by Doping Cu for Enhancing Oxygen Evolution Reaction Activity

Wei Sun^a, Ya Song^b, Xue-Qing Gong^{b,†}, Li-mei Cao^a, Ji Yang^{a,†}Received 00th January 20xx,
Accepted 00th January 20xx

DOI: 10.1039/x0xx00000x

www.rsc.org/

The oxygen evolution reaction (OER) has been regarded as a key half reaction for energy conversion technologies and requires a high energy to create O=O bonds. Transition metal oxides (TMOs) seem to be a promising and appealing solution to the challenge because their diversity of their *d* orbital states. We chose IrO₂ as a model because it is universally accepted as a current state-of-the-art OER catalyst. In this study, copper-doped IrO₂, particularly Cu_{0.3}Ir_{0.7}O₆, is shown to significantly improve the OER activity in acid, neutral and basic solutions compared to un-doped IrO₂. The substituted amount of Cu in IrO₂ has a limit described by the Cu_{0.3}Ir_{0.7}O₆ composition. We determined that the performance of Cu_{0.3}Ir_{0.7}O₆ is due primarily to an increase in the Jahn-Teller effect in the CuO₆ octahedral and partially to oxygen defects in the lattice induced by IrO₆ octahedral geometric structure distortions, which enhance the lift degeneracy of the *t*_{2g} and *e*_g orbitals, making the *d*_{z²} orbital partially occupied. This phenomenon is benign for reducing the difference between ΔG₂ and ΔG₃ in the free energy from the density functional theoretical (DFT) calculations and can yield a lower theoretical overpotential comparable to that of IrO₂. The proposed method of doping foreign elements to tune the electron occupation between the *t*_{2g} and *e*_g orbital states of Ir creates an opportunity for designing effective OER catalysts using the TMO groups.

Introduction

The oxygen evolution reaction (OER) at the anode is the key half reaction for splitting water into H₂ fuel and reducing the CO₂ concentration in fuels (e.g., CO, CH₄) and metal-air batteries¹⁻⁴. However, the OER is a complex process associated with 4e/4H⁺ loss and O=O bond formation, which requires a high overpotential relative to the standard reaction potential (*E*=1.229 V, pH=0) to achieve the desired current density^{1, 5, 6}. The critical step to address the challenge is to find efficient catalysts. One of the most promising catalysts is a transition metal oxide (TMO); this group has nearly infinitely variable properties of its *d* orbital states (*d*⁰~*d*¹⁰)^{7, 8}, particularly *t*_{2g} and *e*_g, which can be systematically modified to optimize the catalytic activity at the surface⁹⁻¹¹. OER catalytic activity of TMOs is governed completely by its *d* orbital electron structure¹²

because the bond making or breaking in OER processes are based on the O-2*p* of intermediates bonding with the M-*nd* of surface sites. Many approaches are been engineered to enhance OER catalytic activity by doping foreign elements into the host structure or modifying the substitute to increase the number of catalytically active sites¹³⁻¹⁸. Numerous studies show that, introducing F¹⁹, Ru^{20, 21}, Ta²² and Zn²³ into IrO₂ can obtain improvement on OER activity. However, there are still important aspects regarding how the doped foreign metals tune the *d* orbital electronic structure of the host element and further affect its OER activity.

Here, we show that copper (Cu) doped IrO₂, particularly in the Cu_{0.3}Ir_{0.7}O₆ composition, exhibits a high OER activity in acid neutral and basic solutions (pH~1, 7 and 13, respectively). We chose IrO₂ as a model because it has been universally accepted as a current state-of-the-art OER catalyst and maintains a stable structure in water oxidation over a broad pH range²⁴⁻²⁷. The copper is taken as dopant due to its special electronic structure (3d¹⁰4s¹), and Cu²⁺ is widely applied in superconductors^{28, 29}. In this study, the Cu that is introduced into the IrO₂ lattice changes the IrO₂ lattice parameters and further affects the *d*-orbital distributions of the Ir-5*d* electrons; these mechanisms are discussed in detail. We also attribute the high performance observed to the fact that the doped Cu changes the Ir site electron structure, lifts its *e*_g orbital and partially occupies its *d*_{z²} orbital.

^aState Environmental Protection Key Laboratory of Environmental Risk Assessment and Control on Chemical Processes, School of Resources and Environmental Engineering East China University of Science and Technology, 130 Meilong Road, Shanghai 200237, P.R. China.

^bKey Laboratory for Advanced Materials, Center for Computational Chemistry and Research Institute of Industrial Catalysis, East China University of Science and Technology, 130 Meilong Road, Shanghai 200237, P.R. China.

[†] yangji@ecust.edu.cn; xgong@ecust.edu.cn.

Electronic Supplementary Information (ESI) available: [Materials, experimental procedures and theoretical calculations; figures including SEM, TEM images, EDS data, EXAFS and XPS spectra, CVs for RHE calibration and polarization curves for mixture of CuO and IrO₂; and tables for EDS and comparison of OER activity]. See DOI: 10.1039/x0xx00000x

Results and Discussion

$\text{Cu}_x\text{Ir}_{1-x}\text{O}_6$ with varying compositions were synthesized hydrothermally via doping different Cu contents into IrO_2 lattice, and crystallized at 600 °C (detailed synthesis information is shown in the Supplementary Information).

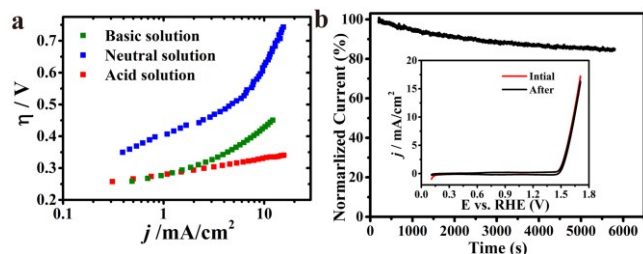


Figure 1. OER activity of $\text{Cu}_{0.3}\text{Ir}_{0.7}\text{O}_6$ in three different pH solutions. (a) Tafel curves of $\text{Cu}_{0.3}\text{Ir}_{0.7}\text{O}_6$. The R in the three solution was $\sim 18\Omega$ (acid), $\sim 15\Omega$ (neutral) and $\sim 28\Omega$ (basic), respectively. (b) Chronoamperometric curves at the constant potential 1.68V vs. RHE. The insert polarization curves for $\text{Cu}_{0.3}\text{Ir}_{0.7}\text{O}_6$ at initial and after chronoamperometric experiments. The catalysts loading were 0.2 mg/cm² on a Ti plate.

Figure 1a shows the electrochemical characterization of the $\text{Cu}_{0.3}\text{Ir}_{0.7}\text{O}_6$ composition³⁰, which exhibited an excellent OER activity in three solutions with different pH values. The η requirements at $j=10$ mA/cm², which is a meaningful reference due to relevant to solar synthesis,³¹ was remarkably small at 351 mV in the acidic solution, 623 mV in the neutral solution and 415 mV in the basic solution for $\text{Cu}_{0.3}\text{Ir}_{0.7}\text{O}_6$, which showed excellent performance in the acidic and neutral solutions and were much smaller compared to some reported effective Co-based catalysts³²⁻³⁴. The excellent performance for $\text{Cu}_{0.3}\text{Ir}_{0.7}\text{O}_6$ was confirmed by measuring the Tafel slope to be ~ 63 mV/dec in the acidic solution, ~ 203 mV/dec in the neutral solution and ~ 105 mV/dec in the basic solution. The stability of the prepared $\text{Cu}_{0.3}\text{Ir}_{0.7}\text{O}_6$ was evaluated by conducting chronoamperometry at 1.68 V (vs. RHE) for 6000s in Figure 1b. In each run, the normalized current slightly decreased due to oxygen bubble buildup on surface, while its CV curves (Figure 1b insert) before and after 6000s are almost identical showing that the catalyst remains stable during OER experiments.

As revealed by nitrogen adsorption isotherms (BET m²/g), the prepared catalysts have close surface areas of 22-30 m²/g (Table.S1). The composition are characterized by EDS and shown in Fig.S1; additional results were listed in Table.S2. Transmission electron microscopy (TEM) showed that Cu-doped IrO_2 had a short rod-like morphology structure that was different from the IrO_2 grain morphology (Fig.S2); this was confirmed by scanning electron microscopy (SEM), as shown in Fig.S3. It should be noted that the doped Cu could change the IrO_2 lattice; thus, we have investigated how doped Cu can affect the IrO_2 rutile structure. The composition was shown to maintain its rutile structure with $x=0\sim 0.3$, and when doped with $x>0.3$, it was found to be a mixture made up of CuO and partially doped IrO_2 . X-ray diffraction (XRD, Fig. 2a) shows the diffraction planes (002) and (111) corresponding to CuO, which peak near $x=0.3$, begin very weakly and increase gradually as more Cu is added,

indicating that $x=0.3$ is the maximum concentration to form solid solution. It was also found that Ir could not insert into the CuO lattice even at a 10% mole ratio due to the different crystal systems present. It also confirm by performing EDX mapping (Fig.S4) shows that Cu homogenously doped in IrO_2 lattice with low Cu composition (for $x=0.1$ and $x=0.3$).

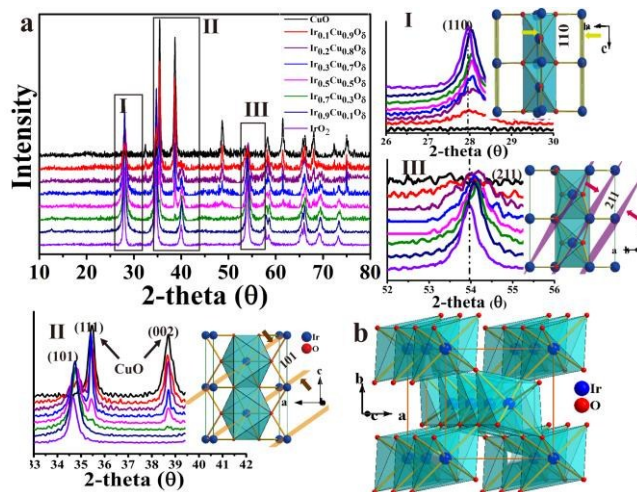


Figure 2. (a) XRD patterns of the $\text{Cu}_x\text{Ir}_{1-x}\text{O}_6$ compositions with different Cu doped amounts. (I), (II) and (III) correspond to the (a) selected area. (b) Polyhedron picture of one IrO_2 cell.

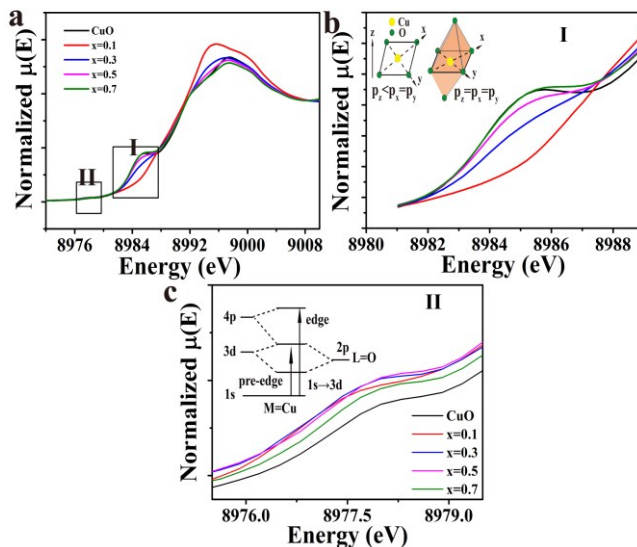


Figure 3. (a) Normalized Cu-K edge XANES spectra for $\text{Cu}_x\text{Ir}_{1-x}\text{O}_6$ compositions. (I) shows the shakedown transition and inset is diagram of Cu-4p orbital energy in two different symmetries, and (II) shows the amplified pre-edge region and inset diagram shows energy level of possible transitions. Both (I) and (II) correspond to the (a) selected area.

These results are confirmed by the Cu-K edge X-ray absorption near-edge structure (XANES), as shown in Fig. 3a. The Cu-K edge of the CuO separated into two regions in the planar symmetry which was a $1s\rightarrow 4p_z$ transition, corresponding to the low energy peak (i.e., the shakedown peak), and $1s\rightarrow 4p_{x,y}$ transitions,

corresponding to the primary edge³⁵. The local symmetry of Cu, however, was changed to an octahedral symmetry as Cu substituted into Ir sites, and the shakedown peak disappeared due to the isotropic $4p$ orbital^{35, 36}. Therefore, no shakedown peak was observed at $x=0.1$ and 0.3 in the XANES, which was confirmed by extended the X-ray adsorption fine structure (EXAFS) of the Cu-K edge shown in Fig.S5. However, the intensity of $x=0.3$ is shown to be above that of $x=0.1$, which indicated that the octahedron might distorted. All of the samples studied showed a weak pre-edge peak, which was assigned to $1s \rightarrow 3d$ due to the quadruple-allowed transition (see Fig. 3a II); this intensity could be achieved by the metal $4p_z$ orbital mixing into the $3d$ orbitals; however, this is not possible due to centrosymmetric complexities³⁵⁻³⁸. A significant feature was also noted: the peak intensity of the doped samples was above that of CuO, indicating the excited distorted of the CuO_6 octahedral at $x=0.3$ and 0.5 .

As shown, the doped Cu produces an elongated IrO_6 octahedron due to the CuO_6 octahedron's strong Jahn-Teller effect^{39, 40}, in which the equatorial four oxygen form a plane that compresses, while the apical oxygen out of plane forms an extended octahedron. The IrO_2 rutile structure exhibits edge sharing along the c axis to form chains, and each chain is linked with four neighboring chains by their shared corners (see Fig. 2b). The Ir-O bonds of the IrO_6 octahedral are not equal⁴¹ ($4L+2S$) and include four longer Ir-O bonds in plane along with two short ones that correspond to the apical O. As mentioned above, as a result of the Jahn-Teller effect of CuO_6 , the apical O in the CuO_6 octahedron is out of plane, compressing the equatorial O of the neighboring Ir site, and compressed Cu-O bonds of the plane likely make the neighboring apical Ir-O bonds longer. The XRD data of the compounds shows that the shift values of the (110) plane, which describes the a axial length, was smaller compared to (101) and (211), which are both represented by a and c axial lengths. This results in the axial ration c/a , a critical parameter for the rutile structure, being decreased compared to that of IrO_2 . The calculated lattice parameters of all samples are listed in Table.S3 based on the XRD data. The performed selected area electron diffraction (SAED) is shown in Fig. S2 and shows that the d -space of the specified planes decreased after Cu doping. The HRTEM of the samples shown in Fig.S6 also revealed that the d -space of the (200) plane was similar between the Cu-doped samples and IrO_2 . The data extracted from the EXAFS (see Fig.S7) of the Ir $-L_{III}$ edge also showed that the Ir-O bond lengths are marginally longer than those of IrO_2 in the samples doped by Cu, while the Ir-Ir peak corresponding to the c axis decreased significantly compared to IrO_2 , indicating a reduced c/a ratio, which is consistent with the XRD and SAED data discussed above. All of these data indicate that the IrO_2 doped by Cu had a significant lattice distortion with elongated Ir-O bonds for apical O and compressed Ir-O bonds for equatorial O.

It has been shown that oxygen vacancies (Vo)^{42, 43} will be generated due to the substituted Cu occupying the lattice site of Ir because the dopant (Cu) charge (+2) is different than the host (Ir) charge (+4); however, the crystal must maintain its electrical neutrality to retain no net charge in the crystal structure; this produces a vacancy. These vacancies are identified and labeled as β by O-1s core level spectrum in Fig.4c. The Fig. 4b shows the

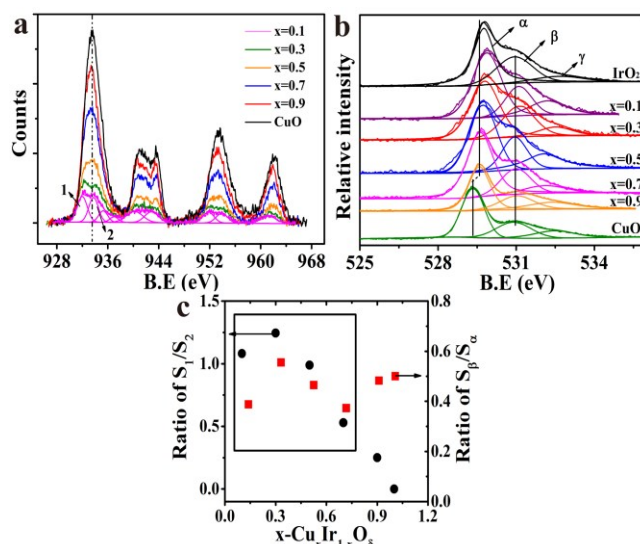


Figure 4. (b) XPS spectra of Cu-2p in $\text{Cu}_x\text{Ir}_{1-x}\text{O}_\delta$ compositions with $x=0.1$ de-convoluted; other compositions' de-convoluted spectra are shown in SI. (c) XPS spectra of O-1s in $\text{Cu}_x\text{Ir}_{1-x}\text{O}_\delta$ compositions. (d) Pattern of the ratio of S_1/S_2 and S_β/S_α versus the doped amount x .

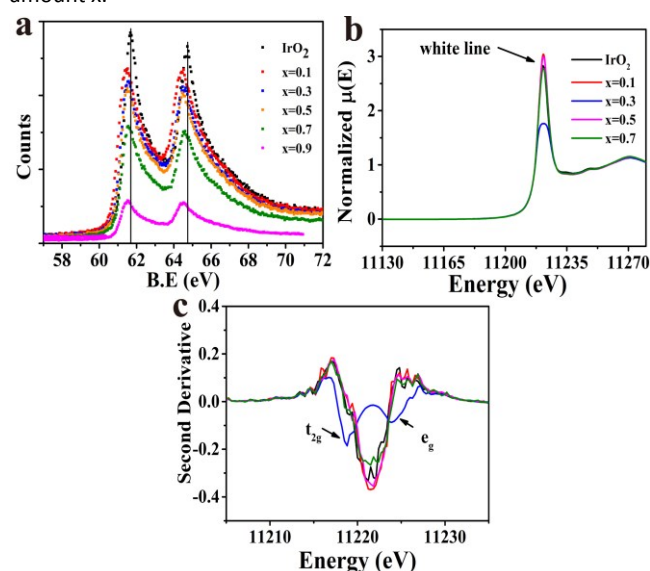


Figure 5. (a) XPS spectra of Ir-4f in $\text{Cu}_x\text{Ir}_{1-x}\text{O}_\delta$ compositions. The solid vertical lines correspond to the Ir-4f_{7/2} and 4f_{5/2} peak position of IrO_2 . (b) Normalized Ir-L_{III} edge XANES spectra for $\text{Cu}_x\text{Ir}_{1-x}\text{O}_\delta$ compositions. (c) Second derivatives of Ir-L_{III} edge XANES spectra for $\text{Cu}_x\text{Ir}_{1-x}\text{O}_\delta$ compositions.

Cu-2p core level spectrum of the doped materials and that of CuO for reference (detail in Fig.S8). It is clearly noted that two de-convoluted peaks were identified and labeled as 1 and 2 at $2p_{3/2}$ in the doped material at $x=0.1$ and 0.3 ; this finding indicated that two different states of the doped Cu corresponded to high and low valence states, respectively. The binding energy of peak 2 was marginally above that of the CuO sample, perhaps corresponding to the O-Cu-O-Ir-O situation. Because the electronegativity of Cu (i.e., the Pauling electronegativity is 1.9) is below that of Ir (i.e., the Pauling electronegativity is 2.2), which meant that oxygen is more

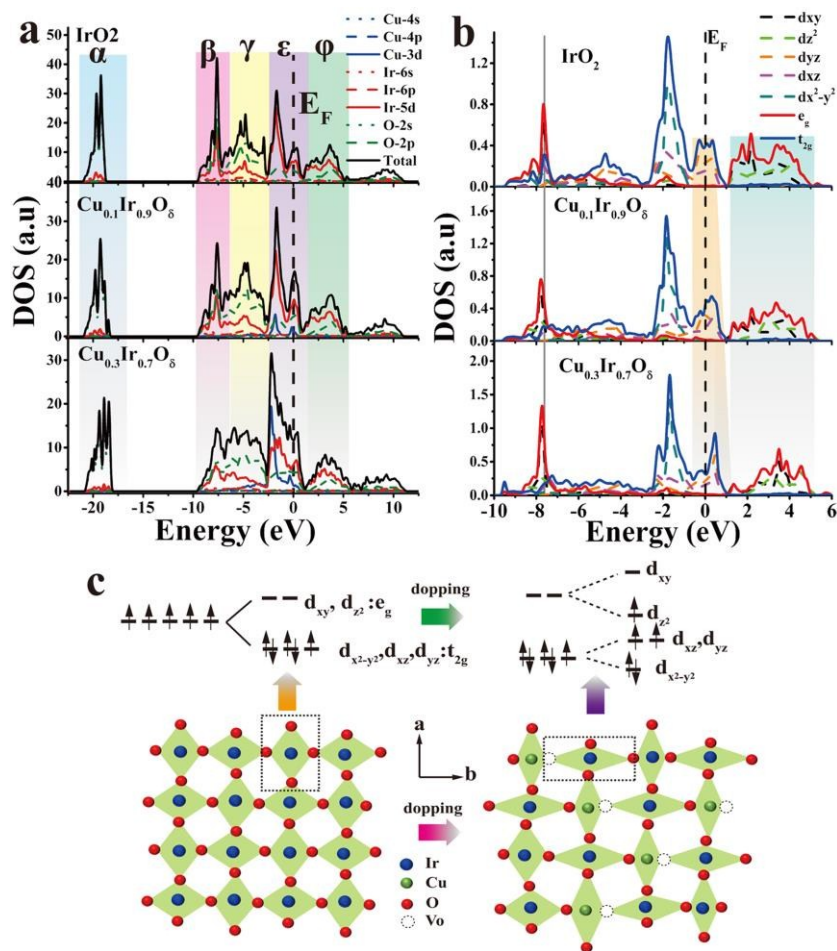


Figure 6. (a) Densities of states for IrO_2 , $\text{Cu}_{0.1}\text{Ir}_{0.9}\text{O}_8$ and $\text{Cu}_{0.3}\text{Ir}_{0.7}\text{O}_8$, the color regions are marked by Greek letters. (b) Partial densities of states for IrO_2 , $\text{Cu}_{0.1}\text{Ir}_{0.9}\text{O}_8$ and $\text{Cu}_{0.3}\text{Ir}_{0.7}\text{O}_8$. (c) Schematic lattice diagram in the ab plane of IrO_2 (left) and substituted by Cu (right). The top row shows Ir-5d orbitals degeneracy of IrO_2 (left) and the lift degeneracy and electrons redistribution by doping Cu.

inclined to gain an electron from copper. This was also confirmed from the O-1s XPS, the primary peak labeled α originated from the metal (Cu,Ir)–O bond in the lattice, and the binding energy progressively decreased with increasing Cu concentration. The ratio of S_1/S_2 and S_β/S_α (i.e., S-peak area) versus the doped amount x is shown in Fig. 4d. It was noted that the variation of S_1/S_2 and S_β/S_α in $\text{Cu}_x\text{Ir}_{1-x}\text{O}_8$ showed similar tendency as the doped amount increased but remained below $x \leq 0.7$; this indicated that there was a strong relationship between the low valence state of the doped Cu and that of the Vo. Thus, we inferred that the oxygen defects were generally closer to the Cu sites. As discussed above, the c -axis of a unit cell by doped Cu was reduced and was directly related to the planar oxygen in the octahedron. Thus, we inferred that the lattice oxygen defects might occur in the plane of the CuO_6 octahedron rather than at the apical location and that the defected position corresponded to the apical O of the IrO_6 octahedron.

This study then investigated how the modified IrO_2 doped by Cu affects the electronic structure of the Ir site. As shown in Fig. 4a (Ir-4f XPS), a shift to a lower binding energy was clearly observed in the doped samples compared to IrO_2 , suggesting a higher electron density at the Ir site. We thus did not assign a low valence to Ir in all samples (see discussion in Fig.S9). The preformed Ir- L_{III} edge XANES (Fig. 4b) revealed that an

increasing number of Ir-5d states were occupied with IrO_2 doped at $x=0.3$ with Cu due to a significant decrease in intensity in the so-called “white line region.” The edge positions of the Ir- L_{III} edge for all of the prepared materials were found to be similar, indicating no valence change on Ir. In the ionic model, the five 5d electrons of the Ir^{4+} ion in IrO_2 were shown to occupy the t_{2g} triplet (i.e., d_{xz} , d_{yz} and $d_{x^2-y^2}$) and leave the higher e_g doublet (i.e., d_{xy} and d_{z^2}) empty under the octahedral crystal field described by the $t_{2g}^5e_g^0$ configuration^{44, 45}. However, as shown in the second derivative spectra (Fig. 5d), only a single feature was observed for IrO_2 due to the IrO_6 octahedron being cross-linked to form a 3D structure; this can be explained by a bond model^{46, 47}. In contrast, the doublet feature was found in some iridate perovskite compositions with the IrO_6 octahedron being regarded as a single cluster. Therefore, Fig. 5c confirms that $x=0.3$ produces a doublet in the white line structure, and other doped compositions yielded results similar to that of IrO_2 . One of surprising features at $x=0.3$ was that the peak intensity and area of the $2p \rightarrow t_{2g}$ ($5d$) transition were increased above those of the $2p \rightarrow e_g$ ($5d$) transition, which are opposite to the findings in iridate perovskites^{46, 47}; thus, we inferred that the e_g state had been partial occupied.

The doped Cu led to an IrO_2 lattice distortion due to the CuO_6 octahedron’s Jahn-Teller effect and also generated oxygen

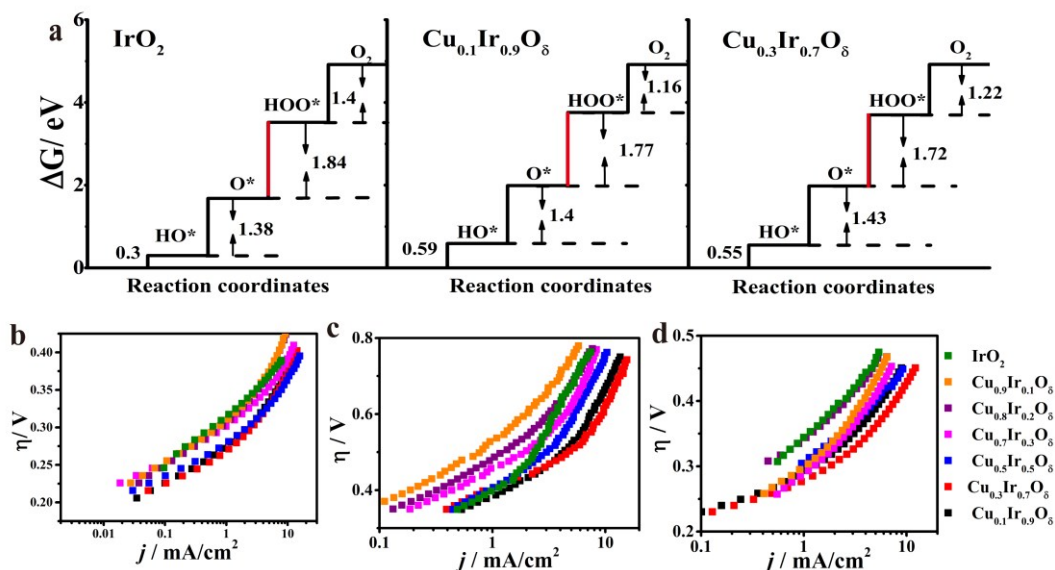


Figure 7. (a) Standard free energy diagram for the OER in IrO₂, Cu_{0.1}Ir_{0.9}O₈ and Cu_{0.3}Ir_{0.7}O₈. (b-d) Tafel plots in acidic, neutral and basic solutions, respectively. The curves are iR-corrected in the acidic (~18 Ω), neutral (~15 Ω) and basic (~28 Ω) solutions, respectively. The catalyst mass loading was ~0.2 mg/cm² for all electrode.

defects, which significantly affected the energy distribution of the *d*-orbitals of Ir sites. The density of states (DOS) is a good descriptor for the bonding character and occupancy of the orbital states⁴⁸⁻⁵¹. Fig. 5a and 5b showed the DOS of IrO₂ and the doped material at $x=0.1$ and 0.3 using the general gradient approximation (GGA) calculation; details of this analysis are shown in the Calculation section of the Support Information. The colored region of Fig. 5a labels α , β , γ , ϵ and ϕ for Ir-O a_{1g} bonding, σ bonding, π bonding, π antibonding (including the non-bonding part) and σ antibonding^{45, 52, 53}. One of the features of DOS is that the σ and π bonding region changed from narrow to relatively broad, and its antibonding states were pulled to a lower energy level as Cu doping increased means weaken the bonding; this was primarily due to the occupancy of σ states. The partial DOS (PDOS) of Ir is shown in Fig. 5b. The d_{xy} orbital occupied states were located at lower energies (gray solid line), while antibonding states moved to higher energies (light blue region) as the Cu doped amount increased, indicating that the d_{xy} orbital was uplifted. In contrast, the d_{z^2} antibonding states were shifted to a lower energy level. The d_{xz} and d_{yz} bands were crossed by the Fermi level (E_F), which changed to a narrow shape and was pushed above E_F , indicating that the bands were empty in the π antibonding orbital; this indicated that the electrons may be half-filled in the d_{xz} and d_{yz} orbital. The $d_{x^2-y^2}$ band showed nearly no variation when fully occupied, even when doped with Cu. As discussed above, the Ir-5*d* electrons showed lifted degeneracy in the octahedron within Cu; this made the d_{z^2} orbital energy decreased, while the d_{xy} orbital energy increased. As a result, an electron might hop to the d_{z^2} orbital (see Fig. 5c), making the e_g orbital partially filled.

Based on the density functional theory (DFT) and the molecular orbital principles, a strong or weak bond formation from a surface site interacting with the reaction intermediates is strongly correlated with the OER activity. A σ bond to a e_g orbital facilitates bonding with oxygen intermediates compared to a π bond t_{2g} orbital due to the e_g orbital's stronger overlap

with O-2*p*^{8, 51, 54}. Suntivch et al.⁵⁴ proposed that e_g occupation close to unity optimizes the rate-determining step (RDS) and thereby leads to a higher OER activity and is successful in perovskite studies. Vojvodic and Nørskov⁵¹ showed that the surface-oxygen bond energy scales with e_g and t_{2g} occupation and has a similar tendency to the interaction between the surface site and O-adsorbate, which becomes weaker with an increasing number of occupied states (e.g., e_g and t_{2g}). The possible OER mechanism on the metal oxides is shown in Fig. S10. The binding free energies of all the reaction intermediates (HO*, O*, HOO*) involved in Fig. S9 are described in Fig. 6a. For a wide class of metal oxides, a linear relationship was found in the binding free energy between OH* and O* equated with $\Delta G_2 + \Delta G_3 = 3.2 \pm 0.2$ eV^{49, 55}. As a result, the catalysts have been optimized, evidenced by the reduction in the difference between ΔG_2 and ΔG_3 . It was found that the sum of ΔG_2 and ΔG_3 met this relationship for IrO₂ (3.22 eV), Ir_{0.9}Cu_{0.1}O₈ (3.17 eV) and Ir_{0.7}Cu_{0.3}O₈ (3.15 eV). In the case of IrO₂ ($t_{2g}^5 e_g^0$), small e_g filling on the Ir sites may result in the electrons of the O-2*p* adsorbate being able to easily hop to the unoccupied σ^* orbital to form Ir-OH and Ir-O bonds, which decrease the free energies of the first and second step (OH* and O*). However, the formation of OOH* will occur at the RDS ($\Delta G_3 = 1.84$ eV) due to the rupture of the surface-oxygen bonds in most of the metal-oxides catalysts. For the IrO₂ doped with Cu ($x=0.1$ and 0.3) with e_g partially filled on the Ir site, it should take a higher energy to form Ir-OH and Ir-O bond ($\Delta G_1 + \Delta G_2 = 1.99$ and 1.98 eV higher 1.68 eV of IrO₂); however, the difference between ΔG_2 and ΔG_3 was found to decrease ($\Delta G_3 - \Delta G_2 = 0.37$ eV and 0.29 eV comparable to 0.46 eV of IrO₂) and reached a lower theoretical overpotential ($\eta_{the}(x=0.3) = 0.39$ eV with $\eta_{the}(x=0) = 0.51$ eV). The experimental data of OER for the studied samples are shown in Fig. 6b-6d, which show that except for Cu_{0.3}Ir_{0.7}O₈, all doped materials exhibited some OER activity; the Cu_{0.2}Ir_{0.8}O₈ and Cu_{0.1}Ir_{0.9}O₈ compositions had a higher j compared to IrO₂ in the basic solutions. In addition, the mechanical mixtures of IrO₂ and

CuO were prepared; however, no improvement in OER activity (see Fig.S11) through mechanical mixing was observed. The η at $j=10$ mA/cm², the Tafel slopes and the mass activities at specific overpotentials in all of the prepared materials are shown in Table.S4. From this table, we can conclude that the doped Cu did enhance the OER activity, and $x=0.3$ showed the excellent performance, which was consistent with the results from the relevant physical characters and DFT calculations.

Conclusions

The relevant experimental and theoretical results clearly showed that the d orbital occupation states of Ir-5d ($t_{2g}^5e_g^0$) in IrO₂ can be tuned by substituting Cu for Ir to create a d_z^2 -antibonding orbital (i.e., one of e_g -antibonding orbitals) that is partially occupied in the Cu_{0.3}Ir_{0.7}O₈ composition. The Cu_{0.3}Ir_{0.7}O₈ composition exhibited an unexpected OER activity from its Tafel slope to its mass activity in three different pH solutions compared to IrO₂. The substitution of Cu in the rutile structure of IrO₂ inherently had a strong Jahn-Teller effect due to the CuO₆ octahedron and induced partial oxygen defects in the lattice that changed the IrO₆ octahedral geometric structure and also lifted degeneracy of the t_{2g} and e_g orbitals. Therefore, the proposed method of doping foreign elements to tune the electron occupation between the t_{2g} and e_g orbital states of Ir sites can yield an opportunity to design effective OER catalysts using TMO group materials.

Acknowledgements

This research is based on work supported by the National Natural Science Foundation of China (21177037, 21277045, 21322307), the Public welfare project of the Ministry of Environmental Protection (201309021), the "Shu Guang" project of the Shanghai Municipal Education Commission and the Shanghai Education Development Foundation, and the Fundamental Research Funds for the Central Universities. We would like to thank beamline BL14W1 (Shanghai Synchrotron Radiation Facility) for providing the beam time.

Notes and references

- N. S. Lewis and D. G. Nocera, *Proc. Natl. Acad. Sci. U.S.A.*, 2006, **103**, 15729-15735.
- H. B. Gray, *Nat. Chem.*, 2009, **1**, 7-7.
- M. G. Walter, E. L. Warren, J. R. McKone, S. W. Boettcher, Q. Mi, E. A. Santori and N. S. Lewis, *Chem. Rev.*, 2010, **110**, 6446-6473.
- J. Chakhalian, A. J. Millis and J. Rondinelli, *Nat Mater*, 2012, **11**, 92-94.
- R. I. Cukier and D. G. Nocera, *Annu. Rev. Phys. Chem.*, 1998, **49**, 337-369.
- S. Hammes-Schiffer, *Acc. Chem. Res.*, 2009, **42**, 1881-1889.
- S.-W. Cheong, *Nat Mater*, 2007, **6**, 927-928.
- J. Suntivich, H. A. Gasteiger, N. Yabuuchi, H. Nakanishi, J. B. Goodenough and Y. Shao-Horn, *Nat. Chem.*, 2011, **3**, 546-550.
- D. W. Jeong, W. S. Choi, S. Okamoto, J.-Y. Kim, K. W. Kim, S. J. Moon, D.-Y. Cho, H. N. Lee and T. W. Noh, *Sci. Rep.*, 2014, **4**.
- J. Chakhalian, J. W. Freeland, H.-U. Habermeier, G. Cristiani, G. Khaliullin, M. van Veenendaal and B. Keimer, *Science*, 2007, **318**, 1114-1117.
- Y. Tokura and N. Nagaosa, *Science*, 2000, **288**, 462-468.
- J. K. Nørskov, T. Bligaard, J. Rossmeisl and C. H. Christensen, *Nat. Chem.*, 2009, **1**, 37-46.
- C. A. Kent, J. J. Concepcion, C. J. Dares, D. A. Torelli, A. J. Rieth, A. S. Miller, P. G. Hoertz and T. J. Meyer, *J. Am. Chem. Soc.*, 2013, **135**, 8432-8435.
- P. Liao, J. A. Keith and E. A. Carter, *J. Am. Chem. Soc.*, 2012, **134**, 13296-13309.
- J. Park, H. Kim, K. Jin, B. J. Lee, Y.-S. Park, H. Kim, I. Park, K. D. Yang, H.-Y. Jeong, J. Kim, K. T. Hong, H. W. Jang, K. Kang and K. T. Nam, *J. Am. Chem. Soc.*, 2014, **136**, 4201-4211.
- B. S. Yeo and A. T. Bell, *J. Am. Chem. Soc.*, 2011, **133**, 5587-5593.
- Q. Zhang, Z. D. Wei, C. Liu, X. Liu, X. Q. Qi, S. G. Chen, W. Ding, Y. Ma, F. Shi and Y. M. Zhou, *Int. J. Hydrogen Energy* 2012, **37**, 822-830.
- D. M. Jang, I. H. Kwak, E. L. Kwon, C. S. Jung, H. S. Im, K. Park and J. Park, *J. Phys. Chem. C*, 2015, **119**, 1921-1927.
- K. S. Kadakia, P. H. Jampani, O. I. Velikokhatnyi, M. K. Datta, S. K. Park, D. H. Hong, S. J. Chung and P. N. Kumta, *J. Power Sources*, 2014, **269**, 855-865.
- S. Siracusano, N. Van Dijk, E. Payne-Johnson, V. Baglio and A. S. Aricò, *Applied Catalysis B: Environmental*, 2015, **164**, 488-495.
- J. Cheng, H. Zhang, G. Chen and Y. Zhang, *Electrochim. Acta*, 2009, **54**, 6250-6256.
- C. Felix, T. Maiyalagan, S. Pasupathi, B. J. Bladergroen and V. Linkov, 2012.
- E. Kuznetsova, V. Petrykin, S. Sunde and P. Krtil, *Electrocatalysis*, 2015, **6**, 198-210.
- C. De Pauli and S. Trasatti, *J. Electroanal. Chem.*, 2002, **538**, 145-151.
- M. Yagi, E. Tomita, S. Sakita, T. Kuwabara and K. Nagai, *J. Phys. Chem. B*, 2005, **109**, 21489-21491.
- Y. Lee, J. Suntivich, K. J. May, E. E. Perry and Y. Shao-Horn, *J. Phys. Chem. Lett.*, 2012, **3**, 399-404.
- Y. Zhao, E. A. Hernandez-Pagan, N. M. Vargas-Barbosa, J. L. Dysart and T. E. Mallouk, *J. Phys. Chem. Lett.*, 2011, **2**, 402-406.
- J. Ghijsen, L. H. Tjeng, J. van Elp, H. Eskes, J. Westerink, G. A. Sawatzky and M. T. Czyzyk, *Phys. Rev. B*, 1988, **38**, 11322-11330.
- R. Fehrenbacher and T. M. Rice, *Phys. Rev. Lett.*, 1993, **70**, 3471-3474.
- A. Minguzzi, F.-R. F. Fan, A. Vertova, S. Rondinini and A. J. Bard, *Chemical Science*, 2012, **3**, 217-229.
- Y. Gorlin and T. F. Jaramillo, *J. Am. Chem. Soc.*, 2010, **132**, 13612-13614.
- M.-R. Gao, X. Cao, Q. Gao, Y.-F. Xu, Y.-R. Zheng, J. Jiang and S.-H. Yu, *ACS Nano*, 2014, **8**, 3970-3978.
- M.-R. Gao, Y.-F. Xu, J. Jiang, Y.-R. Zheng and S.-H. Yu, *J. Am. Chem. Soc.*, 2012, **134**, 2930-2933.
- Y. Liang, Y. Li, H. Wang, J. Zhou, J. Wang, T. Regier and H. Dai, *Nat. Mater.*, 2011, **10**, 780-786.
- J.-H. Choy, D.-K. Kim, S.-H. Hwang and G. Demazeau, *Phys. Rev. B*, 1994, **50**, 16631-16639.

36. L. S. Kau, D. J. Spira-Solomon, J. E. Penner-Hahn, K. O. Hodgson and E. I. Solomon, *J. Am. Chem. Soc.*, 1987, **109**, 6433-6442.
37. J. L. DuBois, P. Mukherjee, A. M. Collier, J. M. Mayer, E. I. Solomon, B. Hedman, T. D. P. Stack and K. O. Hodgson, *J. Am. Chem. Soc.*, 1997, **119**, 8578-8579.
38. J. L. DuBois, P. Mukherjee, T. D. P. Stack, B. Hedman, E. I. Solomon and K. O. Hodgson, *J. Am. Chem. Soc.*, 2000, **122**, 5775-5787.
39. G.-m. Zhao, M. B. Hunt, H. Keller and K. A. Muller, *Nature*, 1997, **385**, 236-239.
40. G. Peralta, D. Puggioni, A. Filippetti and V. Fiorentini, *Phys. Rev. B*, 2009, **80**, 140408.
41. A. A. Bolzan, C. Fong, B. J. Kennedy and C. J. Howard, *Acta Crystallographica Section B*, 1997, **53**, 373-380.
42. J. Wang, Z. Wang, B. Huang, Y. Ma, Y. Liu, X. Qin, X. Zhang and Y. Dai, *ACS Applied Materials & Interfaces*, 2012, **4**, 4024-4030.
43. J. Gan, X. Lu, J. Wu, S. Xie, T. Zhai, M. Yu, Z. Zhang, Y. Mao, S. C. I. Wang, Y. Shen and Y. Tong, *Sci. Rep.*, 2013, **3**.
44. Y. Hirata, K. Ohgushi, J.-i. Yamaura, H. Ohsumi, S. Takeshita, M. Takata and T.-h. Arima, *Phys. Rev. B*, 2013, **87**, 161111.
45. J. Kahk, C. Poll, F. Oropeza, J. Ablett, D. Céolin, J. Rueff, S. Agrestini, Y. Utsumi, K. Tsuei and Y. Liao, *Phys. Rev. Lett.*, 2014, **112**, 117601.
46. J.-H. Choy, D.-K. Kim, G. Demazeau and D.-Y. Jung, *The Journal of Physical Chemistry*, 1994, **98**, 6258-6262.
47. J.-H. Choy, D.-K. Kim, S.-H. Hwang, G. Demazeau and D.-Y. Jung, *J. Am. Chem. Soc.*, 1995, **117**, 8557-8566.
48. B. Hammer and J. K. Nørskov, in *Advances in Catalysis*, ed. H. K. Bruce C. Gates, Academic Press, 2000, vol. Volume 45, pp. 71-129.
49. I. C. Man, H. Y. Su, F. Calle - Vallejo, H. A. Hansen, J. I. Martínez, N. G. Inoglu, J. Kitchin, T. F. Jaramillo, J. K. Nørskov and J. Rossmeisl, *ChemCatChem*, 2011, **3**, 1159-1165.
50. J. Rossmeisl, Z.-W. Qu, H. Zhu, G.-J. Kroes and J. K. Nørskov, *J. Electroanal. Chem.*, 2007, **607**, 83-89.
51. A. Vojvodic and J. K. Nørskov, *Science*, 2011, **334**, 1355-1356.
52. J. S. de Almeida and R. Ahuja, *Phys. Rev. B*, 2006, **73**, 165102.
53. L. F. Mattheiss, *Phys. Rev. B*, 1976, **13**, 2433-2450.
54. J. Suntivich, K. J. May, H. A. Gasteiger, J. B. Goodenough and Y. Shao-Horn, *Science*, 2011, **334**, 1383-1385.
55. S. Piccinin, A. Sartorel, G. Aquilanti, A. Goldoni, M. Bonchio and S. Fabris, *Proc. Natl. Acad. Sci. U.S.A.*, 2013, **110**, 4917-4922.

TOC:

Tuning Ir d-Orbital Occupation via Doping Cu into IrO₂ Lattice to Prepare a Highly Efficient Oxygen Evolution Reaction Catalyst Cu_{0.3}Ir_{0.7}O₆.

